The photonic band structures of body-centred-tetragonal crystals composed of ionic or metal spheres

2000 J. Phys.: Condens. Matter 12 5307

(http://iopscience.iop.org/0953-8984/12/24/319)

J. Phys.: Condens. Matter **12** (2000) 5307–5316. Printed in the UK PII: S0953-8984(00)11565-6

The photonic band structures of body-centred-tetragonal crystals composed of ionic or metal spheres

Weiyi Zhang, Zhenlin Wang, An Hu and Naiben Ming

National Laboratory of Solid State Microstructures and Department of Physics, Nanjing University, Nanjing 210093, China

Received 3 February 2000, in final form 18 April 2000

Abstract. The photonic band structures of body-centred-tetragonal (BCT) crystals composed of ionic or metal spheres are computed using the highly efficient vector-wave Korringa–Kohn–Rostoker (KKR) method; an absolute band gap is found for the photonic crystals with high filling ratio. The band gap is smaller in the crystals composed of ionic spheres than in those composed of metal spheres. The particular BCT structure was chosen since such structure can be easily realized in an electrorheological fluid in the presence of an electric field.

1. Introduction

In the last ten years, intensive research activity has been concentrated on the study of photonic band materials; the interest is focused on the search for dielectric modulated structures in space and seeking for crystal structures and material components which have absolute band gaps. This has been so since Yablonovitch *et al* [1–3] showed that an absolute band gap prohibits the spontaneous emission of light and therefore such photonic crystals can be used to study a wide range of physical problems such as those of light localization [4–5], optical polarizers, optical filters, and micro-cavity lasers [6, 7]; they also have broad potential commercial applications.

The band structures of photonic crystals depend both on the symmetrical properties of the crystal structures and on the materials composing the photonic crystals. Various structures have been considered, and absolute band gaps are found to exist in certain crystal structure types only if the component materials are purely dielectric in character. Thus, recently effort has shifted in the following two directions: (1) attempts to further lower the point symmetry of the composite material [8, 9]; (2) attempts to explore other material composites [10–12]; the aim is to optimize the combination of these two factors so that the band-gap/mid-gap frequency can be maximized. As is well known in electronic band-structure calculations, the band gap is determined by the Fourier component of the potential modulation in space; this depends not only on the contrast between the two materials making up the photonic crystals, but also depends on their filling ratios. Since the metallic component has a negative real part, the contrast between the metallic component and usual dielectric media can reach a maximum value when they form photonic crystals [13, 14].

In this paper, we will study photonic crystals composed of ionic or metal spheres embedded in dielectric media. We will concentrate on body-centred-tetragonal (BCT) structures since a BCT structure can be easily realized in an electrorheological fluid of metallic coated spheres in the presence of an external electric field [15]. The dielectric functions of ionic and metallic materials are frequency dependent and have a frequency window in which the electromagnetic

0953-8984/00/245307+10$30.00

wave cannot propagate in the bulk material; thus it is hoped that photonic crystals composed of such materials will be more suited to forming absolute photonic band gaps. While it is already known that BCT crystals composed of purely dielectric media do not have absolute band gaps, we show that BCT crystals composed of ionic or metal spheres embedded in dielectric media do have sizable absolute band gaps and have potential industrial applications.

Because of the existence of a frequency window for the expulsion of electromagnetic waves from such materials, one expects a sharp change in the electric field at the interface when the frequency falls into these windows. To deal with such a situation, one needs a numerical method which can incorporate the interface boundary condition accurately; instead of expanding the electromagnetic wave in reciprocal space as the usual plane-wave methods do [16–18], one needs to expand the electromagnetic field in real space so that the real-space boundary condition can be easily incorporated. This is the so-called Korringa–Kohn–Rostoker (KKR) method [19, 20], which was first put into practice in electronic band-structure calculations some decades ago. Recently, the vector-wave KKR method has been formulated for electromagnetic waves propagating in photonic crystals [21–28]; also we have written a very efficient program code based on the vector-wave KKR method and tested it on a variety of previous known results: fast convergence and high accuracy have been proved for all cases. The advantage of the vector-wave KKR method is most obvious for photonic crystals with metallic components; comparison of diamond structures made of ideal metal spheres embedded in dielectric media shows that the vector-wave KKR method needs much less CPU time and memory space than the finite-difference time-domain method [29]. This method will be used in this paper.

The rest of the paper is organized as follows. In section 2, the vector-wave KKR method is physically derived from the scattering picture; a short comparison with other methods is made and its advantages are discussed. The numerical accuracy and high convergence rate of the vector-wave KKR method are demonstrated. The photonic band structures of various BCT crystals are presented and discussed in section 3 for different component elements and filling ratios. Section 4 gives our conclusions.

2. The vector-wave Korringa–Kohn–Rostoker method

The photonic band structures are obtained by solving the Maxwell equations for photonic crystals; the photonic crystals are usually prepared by embedding one dielectric material in a background medium, and the dielectric difference between the embedded and background media reflects a scattering potential for the electromagnetic wave propagating in the media. In usual photonic crystals, such scattering potentials can be viewed as sums of potentials for isolated scatterers; this is where the vector-wave KKR method finds application [19, 20]. In the vector-wave KKR method, the electric field in the vicinity of the scatterer i can be expressed as the sum of the incoming and outgoing waves with respect to scatterer i. Therefore, one has to study the scattering properties of each of the scatterers first, since the scattering properties of the whole photonic crystal result from these individual scattering processes.

Let us consider one spherical scatterer i with radius r_S and study the scattering property of a partial wave with angular momentum l, projection of the angular momentum m, and polarization of the field σ. Assume that the incident wave has amplitude one with respect to the vector spherical harmonics $\vec{J}_i^{lm\sigma}(\vec{r})$. The index i reflects the fact that we use the local basis with its origin at the scatterer i for the field nearby. The outgoing wave is similarly expressed using the vector spherical harmonics $\vec{H}_i^{lm\sigma}(\vec{r})$. The amplitudes of outgoing waves are related to that of the incident wave by the boundary condition for the electromagnetic wave at the sphere surface; the amplitudes of outgoing waves make up the so-called scattering T-matrix

if the amplitude of the incident wave is set to 1. The sums of the incident and outgoing waves together determine the electromagnetic field outside the scattering region ($r > r_S$):

$$\vec{E}_i(\vec{r}) = \sum_{lm\sigma}[\vec{J}_i^{lm\sigma}(\vec{r}) + t_i^{lm\sigma}\vec{H}_i^{lm\sigma}(\vec{r})]a_i^{lm\sigma}$$

with $a_i^{lm\sigma}$ denoting the amplitude of the incident wave. This is all that we need if we are only interested in the field outside the scattering region.

Once the problem for a single scatterer is solved, the many-scatterer problem can be studied in the same way. Now let us assume that the photonic crystals contain N scatterers and take a look at the particular scatterer i. In this case, the incident wave for the scatterer i located at $\vec{R}_i$ contains two parts; one part comes from the external incident wave $b_i^{lm\sigma}$ from outside of the crystal and the other comes from the outgoing waves emanating from the rest of the scatterers in the crystals. Therefore, the total incident wave for the scatterer i can be written as the sum of these two terms:

$$\sum_{lm\sigma} a_i^{lm\sigma}\vec{J}_i^{lm\sigma}(\vec{r}-\vec{R}_i) = \sum_{lm\sigma} b_i^{lm\sigma}\vec{J}_i^{lm\sigma}(\vec{r}-\vec{R}_i) + \sum_{lm\sigma;\,j\neq i} a_j^{lm\sigma}t_j^{lm\sigma}\vec{H}_j^{lm\sigma}(\vec{r}-\vec{R}_j).$$

Here the indices i and j take the values from 1 to N, so a linear set of equations are obtained which relate the amplitudes of the different scattering regions. Once these amplitudes are determined, so is the electromagnetic wave in the crystals outside the scattering regions. The equation set derived above can be further simplified after applying the addition theorem for the vector spherical harmonics to move the centre of coordinates to the same origin. The equation set governing the coefficients a finally takes the form [21, 26–28]

$$\left[\delta_{ss'}\delta_{ll'}\delta_{mm'}\delta_{\sigma\sigma'} - \sum_{l''m''\sigma''} G^{ss'}_{lm\sigma;l'm'\sigma'}(\vec{k})t^{s'}_{l'm'\sigma'}\right]a^{l'm'\sigma'}_{s'} = b^{lm\sigma}_{s}. \tag{1}$$

Here we have carried out a Fourier transformation to the momentum space; $\vec{k}$ is the Bloch wavevector and s is the index of the scatterer in the primary cell. $G^{ss'}_{lm\sigma;l'm'\sigma'}(\vec{k})$ is the Fourier transform of the structure factor, which can be expressed as

$$G^{ij}_{lm\sigma;l'm'\sigma'}(\vec{R}) = \begin{cases} \displaystyle\sum_{\mu} C(l1l;\, m{-}\mu\mu)g_{lm-\mu;l'm-\mu'}C(l'1l';\, m'{-}\mu\mu) \\ \qquad \text{for } \sigma = \sigma' \\ \displaystyle\sqrt{\frac{2l'+1}{l'+1}}\sum_{\mu} C(l1l;\, m{-}\mu\mu)g_{lm-\mu;l'-1m-\mu'}C(l'-11l';\, m'{-}\mu\mu) \\ \qquad \text{for } \sigma = m \text{ and } \sigma' = e \\ \displaystyle -\sqrt{\frac{2l'+1}{l'+1}}\sum_{\mu} C(l1l;\, m{-}\mu\mu)g_{lm-\mu;l'-1m-\mu'}C(l'-11l';\, m'{-}\mu\mu) \\ \qquad \text{for } \sigma = e \text{ and } \sigma' = m. \end{cases} \tag{2}$$

C is the Clebsch–Gordon coefficient for the angular momenta 1 and l, which combines the vector nature of the electromagnetic wave and the space dependence of the electromagnetic wave. g is the scalar structure factor:

$$g_{lml'm'} = 4\pi\sum_{l''m''} \mathrm{i}^{l-l'-l''}C_{lm;l'm';l''m''}h_{l''}(\kappa R)Y^*_{l''m''}(-\hat{R})$$

where $\mathrm{i} = \sqrt{-1}$ and $\kappa = \omega/c$. $C_{lml'm'l''m''}$ are the so-called Gaunt coefficients which determine the coefficient of overlap among the three spherical harmonics (l, m), (l', m'), and (l'', m''). h_l and Y_{lm} are the usual first-kind Hankel functions and spherical harmonics, respectively.

Since the frequency enters into the structure factor, the matrix equation of the vector-wave KKR method is a set of highly nonlinear equations with respect to the frequency. However, the physical solution of the above equation set can be picked out by counting the number of positive pseudo-eigenvalues for each frequency. Thus the original problem of obtaining the eigenfrequencies is reduced to that of searching for the change in the number of positive pseudo-eigenvalues as a function of the frequency, and the degeneracy of the eigenfrequency is determined by the counter-change in the number of neighbouring pseudo-eigenvalues. The accuracy of the solution is set by the resolution of the frequency mesh points and the value of l; we generally require the eigenfrequency to be accurate to the third digit. Our program code has been tested extensively with other available results; even for structures composed of ideal metal spheres, our band structures are in excellent agreement with that calculated using the finite-difference time-domain method [29] with the finest mesh size possible.

3. Numerical results and discussion

The photonic band gap depends both on the crystal symmetry and on the symmetry and composition of the embedded elements; we will concentrate in this paper on the body-centred-tetragonal (BCT) structures composed of spheres in a constant background of dielectric material. The background dielectric constant is set to 1 for simplicity, as the spectra for other background dielectric constants can be deduced easily using the scaling relation. The spheres considered can be of either ionic or metallic nature; there can be a single layer or a double layer of the two component elements. Using a double layer of spheres also has relevance to the experimental situation for photonic crystals, because metal spheres are usually coated with dielectric layers in order to avoid current formation. The reason for considering BCT photonic crystals is that such structures can be easily realized in an electrorheological fluid of metallic coated spheres [15]; thus it is possible to manufacture photonic crystals with optical wavelengths. The particular BCT lattice type that we have in mind has the lattice constant $\tilde{c} = c/a = \sqrt{2/3}$; this structure has a chain-like arrangement when the spheres touch each other on the z-axis. There, the maximum filling ratio also takes a higher value (of $f = 0.698$) than that for body-centred-cubic (BCC) crystals.

We have used our recently developed vector-wave KKR program code to compute the various structures with different elements mentioned above. Our results demonstrate that while these structures do not favour the formation of absolute band gaps for crystals composed of purely dielectric spheres, an absolute photonic band gap does occur if ionic or metal spheres are used. The photonic band structures of BCT crystals are calculated along the high-symmetry points; their coordinates in the first Brillouin zone are: X$(1/2, 1/2, 0)$; M$(1, 0, 0)$; $\Gamma(0, 0, 0)$; H$(0, 0, (1+\tilde{c}^2)/2\tilde{c})$; and H$(1, 0, (1-\tilde{c}^2)/2\tilde{c})$ in units of $2\pi/a$, where a is the lattice constant on the x–y plane. Note that if $\tilde{c} = 1$, the BCT structure is reduced to a BCC structure; then points H and H$'$ become equivalent to each other. The sphere filling ratio is given by $f = (8\pi/3\tilde{c})(r_S/a)^3$; the photonic band structures are all calculated with the angular momentum $l = 7$. Our numerical study reveals an indirect gap between the Γ point in the conduction band and the M point in the valence band in all these structures. While the absolute band gap depends on the proper choice of the material parameters for the ionic spheres, it is quite general for the structures composed of metal spheres.

We first consider photonic crystals composed of ionic materials. In the bulk ionic materials there is strong coupling between the transverse optical phonon modes and the external electromagnetic wave; the resulting mixed modes are called polaritons, which appear either in the frequency range below the transverse optical phonon frequency ω_T or in that above the longitudinal optical phonon frequency ω_L. Thus, the electromagnetic wave cannot propagate

into the forbidden gap between the transverse and longitudinal optical phonon frequencies in bulk ionic crystals. The situation changes in the case of photonic crystals composed of ionic spheres due to the presence of resonance modes of the spheres [30] and due to the connected network of voids in the background media—so the electromagnetic wave can in principle propagate. According to Fuchs and Kliewer [30], the resonance modes of the ionic spheres can be found by applying the divergence condition to the scattering T-matrix, and they can be classified as: the low-frequency modes below ω_T, the surface modes between ω_T and ω_L, and the high-frequency modes above ω_L. The low- and high-frequency modes are bulk modes because the dielectric constants in these frequency ranges are positive; between the transverse and longitudinal optical phonon frequencies, the dielectric constants are negative, so electromagnetic waves cannot penetrate into the interior of the ionic spheres, and thus form surface modes. However, only the low-frequency and surface modes have rather sharp resonance peaks, while the high-frequency modes have only broader peaks; the sharp resonance modes drastically modify the behaviour of photon propagation in such media, as we shall see below. We have computed the photonic structures of two different materials; one is GaAs and another is MgO. GaAs has only a very small polariton gap while MgO has a quite large polariton gap; an absolute band gap is found to exist only in MgO and its size is directly correlated with the size of the polariton gap. Thus we will take MgO as our example in the following discussion; its material parameters are: dielectric constant $\epsilon(\infty) = 2.95$; longitudinal frequency $\omega_L = 14\times10^{13}\ \mathrm{s}^{-1}$; and transverse frequency $\omega_T = 7.5\times10^{13}\ \mathrm{s}^{-1}$. The general dielectric function for ionic spheres is assumed to be a real number and takes the form

$$\epsilon(\omega) = \epsilon(\infty)(\omega_L^2 - \omega^2)/(\omega_T^2 - \omega^2).$$

We take the lattice constant $a = 7.54\ \mu$m [17], so the dimensionless parameters used in the numerical computation are $\omega_L a/2\pi c = 0.56$ and $\omega_T a/2\pi c = 0.30$.

The photonic band structure for the filling ratio $f = 0.69$ is displayed in figure 1(a), The densely distributed bands below the transverse optical phonon frequency $\omega_T a/2\pi c = 0.3$ are contributed by the low-frequency resonance modes of ionic spheres, while those below the longitudinal optical phonon frequency $\omega_L a/2\pi c = 0.56$ are caused by the surface resonance modes [30]. One notable feature is the existence of two rather dispersive bands between these two batches of flat bands; these bands are identified as the bands of propagation among the voids, since they persist when the filling ratio becomes very small. The absolute band gap is an indirect gap between the M point of the upper densely distributed bands and the Γ point of the propagation band; the mid-gap frequency and gap/mid-gap frequency are $\omega a/2\pi c = 0.373$ and 0.093, respectively. As the size of the ionic sphere radius decreases, the number of flat bands in the lower and upper frequency ranges decreases, and the dispersion of the propagation band becomes large, which makes the band gap smaller. In fact, the absolute band gap disappears below the filling ratio $f = 0.6$ due to the high dispersion of the propagation band. The photonic band structures for ionic spheres with 5% high-dielectric-constant coating (with $\epsilon = 12$) are shown in figure 1(b); the filling ratios are $f = 0.698$ and $f = 0.598$ for the coated and uncoated ionic spheres, respectively. The absolute band gap and number of flat bands are both reduced because of the reduction of the ionic sphere radius; the high-dielectric-constant coating layer also pulls down the frequency of the whole spectrum, since it acts as an attractive potential for the electromagnetic wave. The mid-gap frequency and gap/mid-gap frequency are 0.356 and 0.067, respectively. Note that the combination of the ionic and high-dielectric-constant materials favours the formation of a band gap, since a pure ionic sphere with the filling ratio $f = 0.6$ has no absolute band gap.

For the photonic crystals composed of metal spheres, the dielectric function of the plasmon model is adopted, $\epsilon(\omega) = 1 - \omega_p^2/\omega^2$ with ω_p denoting the plasmon frequency. Just like in

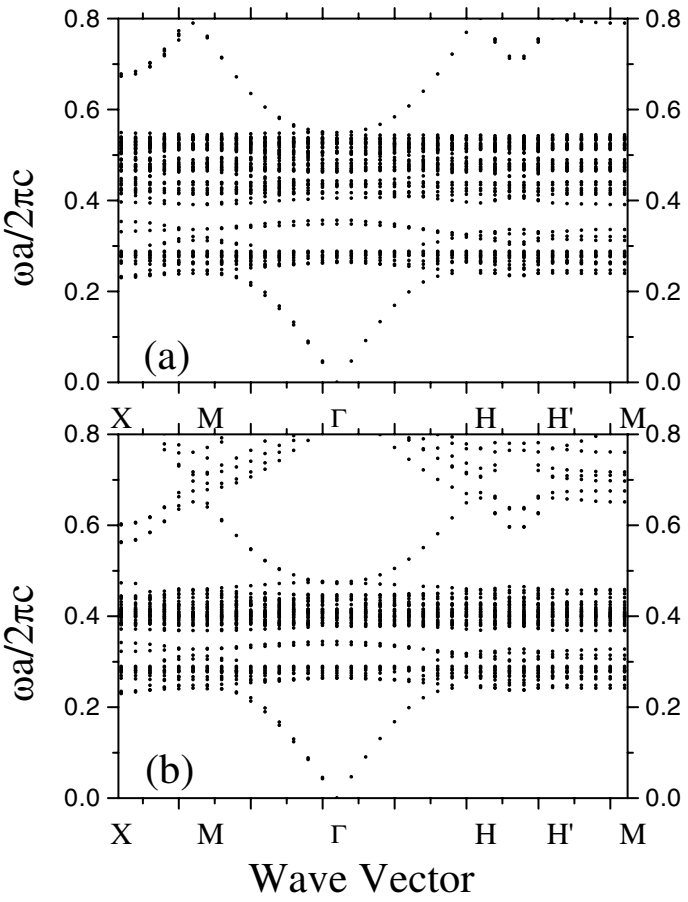

Figure 1. The photonic band structures of BCT crystals composed of ionic spheres in air: (a) purely ionic spheres with the material parameters $\epsilon(\infty) = 2.95$, $\omega_L a/2\pi c = 0.56$, $\omega_T a/2\pi c = 0.30$, and $f = 0.69$; (b) coated ionic spheres with coating of thickness 5% of the total radius and dielectric constant $\epsilon = 12$, and $f = 0.698$.

the case of ionic spheres, the resonance modes of metal spheres are also determined from the zeros of the denominator of the scattering T-matrix. In contrast to the ionic situation, the dielectric constant is always negative below the plasmon frequency and positive above; therefore the only resonance modes of the metal spheres below the plasmon frequency are the surface resonance modes. These surface resonance modes are called Mie resonance modes; they are determined by the condition $\epsilon = -(l+1)/l$ when the radius of the metal spheres approaches zero [30]. The corresponding frequency is then given by $\omega_l = \omega_p\sqrt{l/(2l+1)}$. The frequency of the Mie surface resonance for finite radius, however, is reduced [30]. In figure 2(a), the photonic band structures for the reduced plasmon frequency $\omega_p a/2\pi c = 0.5$ and filling ratio $f = 0.69$ are shown. When the frequency is higher than the reduced plasmon frequency 0.5, the overall photonic structures very much resemble the structures in the vacuum; the most significant change from the vacuum spectrum takes place at the surface Mie-resonance frequency ω_l, where the width of the Mie-resonance-induced bands increases with the size of the metal spheres because of the overlapping among the neighbouring modes. Well below the surface Mie-resonance frequency ω_l, an absolute band gap opens up between the Γ point of

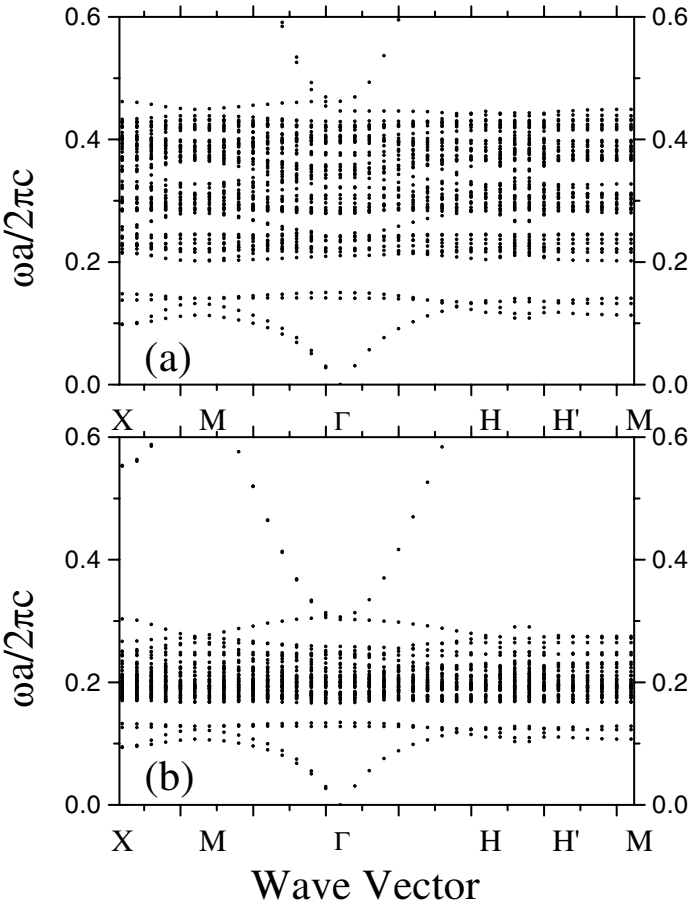

Figure 2. The photonic band structures of BCT crystals composed of metal spheres in air: (a) purely metal spheres with the material parameters $\omega_p a/2\pi c = 0.5$ and $f = 0.69$; (b) coated metal spheres with coating of thickness 5% of the total radius and dielectric constant $\epsilon = 12$, and $f = 0.698$.

the fourth band and the M point of the fifth band; the mid-gap frequency and gap/mid-gap frequency are 0.176 and 0.292. Our calculation suggests that the size of the gap monotonically decreases as the filling ratio decreases, and vanishes when the filling ratio $f \leqslant 0.5$. The higher filling ratio of metal spheres restricts the space in which electromagnetic wave can propagate; an absolute band gap results from strong squeezing of the field. For the metal spheres with a high-dielectric-constant ($\epsilon = 12$) coating, the photonic band structure is shown in figure 2(b); the coating thickness is 5% of the whole sphere's radius and the filling ratio of the whole sphere is $f = 0.698$. It is seen that the Mie-resonance-related bandwidth shrinks and the photonic band gap decreases as the filling ratio of the metal spheres is reduced to $f = 0.598$; the mid-gap frequency and gap/mid-gap frequency become 0.151 and 0.219, respectively. If the metal spheres are not coated with high-dielectric-constant material, the photonic band gap is even smaller.

The above band structures actually correspond to a very small lattice constant or very poor metals; otherwise the reduced plasmon frequency is usually much larger, in view of the current engineering techniques for making the photonic crystals. To improve the relevance to

the experimental situation, we also consider a sample composed of aluminium spheres. The plasmon frequency is $\omega_p = 15.3$ eV, and if we take the lattice constant $a = 1.2$ μm, the reduced plasmon frequency is $\omega_p a/2\pi c = 14.8$. The calculated photonic band structures are shown in figure 3(a); the characteristic feature of the band structures is the large band gaps in all directions, but the absolute band gap is actually much smaller. The absolute band gap is also an indirect gap between the Γ point in the fourth band and the M point in the fifth band; the mid-gap frequency and gap/mid-gap frequency are 0.806 and 0.218, respectively. Because the reduced plasmon frequency is so high, the corresponding Mie resonances lie high above the band gap. Comparing figure 2(a) and figure 3(a), we find that the dispersions of the conduction and valence bands are both sensitive functions of the reduced plasmon frequency; the higher the reduced plasmon frequency, the larger the dispersion. The photonic band structure for metal spheres coated with high-dielectric-constant ($\epsilon = 12$) material is shown in figure 3(b). The coating layer thickness and the filling ratio for the whole sphere are the same as for figure 2(b); the mid-gap frequency and gap/mid-gap frequency are 0.674 and 0.162. Again the absolute band gap is shrunken due to the smaller filling ratio for metal spheres.

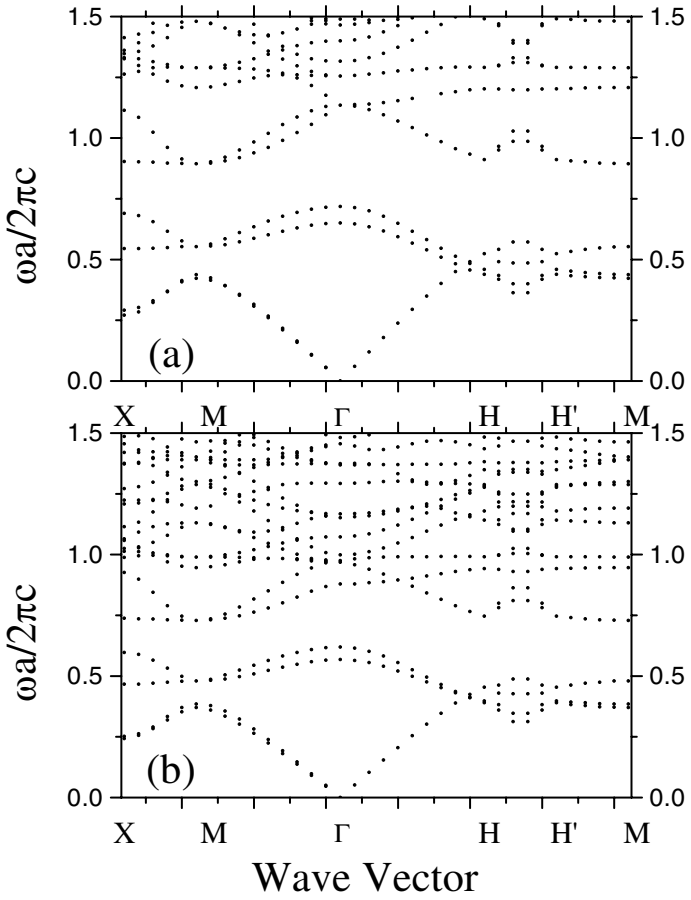

Figure 3. The photonic band structures of BCT crystals composed of metal spheres in air: (a) purely metal spheres with the material parameters $\omega_p a/2\pi c = 14.8$ and $f = 0.69$; (b) coated metal spheres with coating of thickness 5% of the total radius and dielectric constant $\epsilon = 12$, and $f = 0.698$.

For the range of frequencies much lower than the plasmon frequency ω_p, the dielectric constant is a large negative number, and can thus be modelled by a large negative constant. Comparative study of photonic band structures using the plasmon model and a negative large constant shows that the overall structures are the same except some fine details. These are illustrated in figure 4; all parameters are the same as those of figure 3 except that the dielectric function of the metal spheres is replaced by a large negative constant, $\epsilon = -200$. In the photonic crystal with single-layer metal spheres, the mid-gap frequency and gap/mid-gap frequency are 0.777 and 0.244; in the case of metal spheres coated with high-dielectric-constant material, the mid-gap frequency and gap/mid-gap frequency are 0.639 and 0.172, respectively.

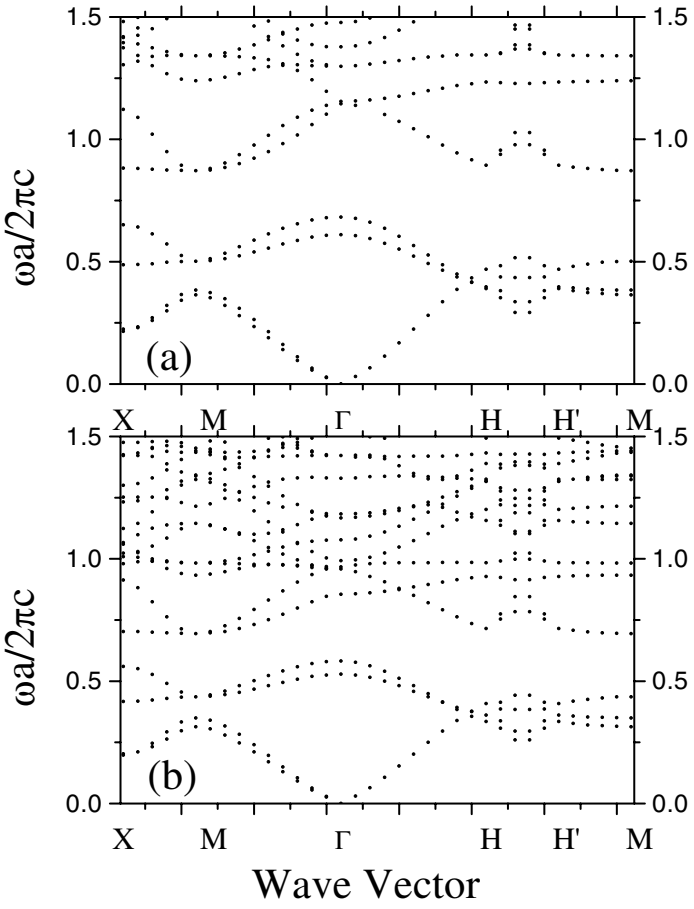

Figure 4. The photonic band structures of BCT crystals of metal spheres in air: (a) purely metal spheres with the material parameters $\epsilon = -200$ and $f = 0.69$; (b) coated metal spheres with coating of thickness 5% of the total radius and dielectric constant $\epsilon = 12$, and $f = 0.698$.

Finally, we would like to mention that the convergence and accuracy of our program code have been fully checked against other numerical methods. In the case of diamond crystal composed of ideal metal spheres with filling ratio $f = 0.3103$ embedded in a dielectric medium with $\epsilon = 2.1$, our photonic band structure for $l = 7$ is in perfect agreement with that calculated by the finite-difference time-domain method [29]; our gap/mid-gap frequency (0.5558) lies between the best available value (0.5333) and the asymptotic value (0.5619).

4. Conclusions

In summary, we have studied in this paper the photonic band structures of BCT crystals composed of spheres; the spheres can be either ionic or metallic materials. In all the structures studied, we found an absolute band gap. The gap is particularly large for the structures composed of metal spheres. This is important in view of the fact that crystals composed of purely dielectric spheres have no absolute band gap at all. These results show that our newly developed program code using the vector-wave KKR method offers a reliable and efficient way to calculate photonic band structures for dielectric as well as metallic systems.

Acknowledgments

We acknowledge with thanks the allocation of CPU time on the SGI ORIGIN 2000 of the Laboratory of Computational Condensed Matter Physics. The present work was supported in part by the National Natural Science Foundation of China under Grants No NNSF 19677202 and No NNSF 19674027. The partial financial support from the key research project in the 'Climbing Programme' of the National Science and Technology Commission of China is also warmly acknowledged.

References

[1] Yablonovitch E 1987 *Phys. Rev. Lett.* **58** 2059
[2] Yablonovitch E, Gmitter T J and Bhat R 1988 *Phys. Rev. Lett.* **61** 2546
[3] Yablonovitch E and Gmitter T J 1989 *Phys. Rev. Lett.* **63** 1950
[4] Zhang Z Q, Wong C C, Fung K K, Ho Y L, Chan W L, Kan S C, Chan T L and Cheung N 1998 *Phys. Rev. Lett.* **81** 5540
[5] Kuzmiak V and Maradudin A A 1998 *Phys. Rev.* B **57** 15 242
[6] Wang Tairan, Moll N, Cho Kyeongjae and Joannopoulos J D 1999 *Phys. Rev. Lett.* **82** 3304
[7] Szymanska M H, Hughes A F and Pike E R 1999 *Phys. Rev. Lett.* **83** 69
[8] Busch K and John S 1999 *Phys. Rev. Lett.* **83** 967
[9] Li Zhiyuan, Gu Benyuan and Yang Guozhen 1998 *Phys. Rev. Lett.* **81** 2574
[10] Tarhan I I and Watson G H 1996 *Phys. Rev. Lett.* **76** 315
[11] Vos W L *et al* 1996 *Phys. Rev.* B **53** 16 231
[12] Busch K and John S 1998 *Phys. Rev.* B **58** 3896
[13] Yannopapas V, Modinos A and Stefanou N 1999 *Phys. Rev.* B **60** 5359
[14] Kuzmiak V and Maradudin A A 1997 *Phys. Rev.* B **55** 7427
[15] Wen W, Wang N, Ma H, Lin Z F, Tam W Y, Chan C T and Sheng P 1999 *Phys. Rev. Lett.* **82** 4248
[16] Zhang Z and Satpathy S 1990 *Phys. Rev. Lett.* **65** 2650
[17] Sigalas M M, Soukoulis C M, Chan C T and Ho K M 1994 *Phys. Rev.* B **49** 11 080
[18] Meade R D, Rappe A M, Brommer K D, Joannopoulos J D and Alerhand O L 1993 *Phys. Rev.* B **48** 8434
[19] Korringa J 1947 *Physica* **13** 392
[20] Kohn W and Rostoker N 1954 *Phys. Rev.* **94** 1111
[21] Ohtaka K 1979 *Phys. Rev.* B **19** 5057
Ohtaka K 1980 *J. Phys. C: Solid State Phys.* **13** 667
[22] Ohtaka K and Tanabe Y 1996 *J. Phys. Soc. Japan* **65** 2265
[23] Ohtaka K and Tanabe Y 1996 *J. Phys. Soc. Japan* **65** 2276
[24] Ohtaka K and Tanabe Y 1996 *J. Phys. Soc. Japan* **65** 2670
[25] Ohtaka K, Ueta T and Tanabe Y 1996 *J. Phys. Soc. Japan* **65** 3068
[26] Wang X D, Zhang X-G, Yu Q L and Harmon B N 1993 *Phys. Rev.* B **47** 4161
[27] Moroz A 1995 *Phys. Rev.* B **51** 2068
Moroz A 1994 *J. Phys. C: Solid State Phys.* **6** 171
[28] Stefanou N, Yannopapas V and Modinos A 1998 *Comput. Phys. Commun.* **113** 49
[29] Fan S, Villeneuve P R and Joannopoulos 1996 *Phys. Rev.* B **54** 11 245
[30] Fuchs R and Kliewer K L 1968 *J. Opt. Soc. Am.* **58** 319